Supporting Information

Two-step strategy improves the wide-temperature-range thermoelectric performance of $Mg_{3+x}Bi_{1.29}Sb_{0.7}Te_{0.01}$

Yushuo Ma [a,1] , *Xiao-Lei Shi* [b,1], *Li Zhang* [*a], *Han Gao* [c], *Meng Li* [b], *Liang-Cao Yin* [d], *Wei-Di Liu* [b], *Qingfeng Liu* [d], *Yan-Ling Yang* [a], *Zhi-Gang Chen* [*b]

[a] School of Materials Science and Engineering, Shaanxi University of Science & Technology, Xi'an 710021, China.

[b] School of Chemistry and Physics, ARC Research Hub in Zero-emission Power Generation for Carbon Neutrality, and Centre for Materials Science, Queensland University of Technology, Brisbane, Queensland 4000, Australia.

[c] Key Laboratory of Material Physics of Ministry of Education, School of Physics and Microelectronics, Zhengzhou University, Zhengzhou 450052, China.

[d] State Key Laboratory of Materials-Oriented Chemical Engineering, College of Chemical Engineering, Nanjing Tech University, Nanjing 211816, China.

[1] These two authors contribute equally.

[*] Corresponding author e-mails: zhangli@sust.edu.cn (L. Zhang), zhigang.chen@qut.edu.au (Z.-G. Chen).

1. Materials and Methods

Material synthesis: Under argon protection in a glovebox with oxygen and water content below 0.1 ppm, high-purity magnesium powders (Mg, 99.5%, Alfa Aesar), bismuth powders (Bi, 99.99%, Alfa Aesar), antimony powders (Sb, 99.99%, Alfa Aesar), and tellurium powders (99.999%) were weighed according to the nominal stoichiometry of $Mg_{3+x}Bi_{1.29}Sb_{0.7}Te_{0.01}$ (x = 0.2, 0.3, 0.4, 0.5). All elements were loaded into a stainless-steel jar and mixed for 15 minutes without grinding balls, followed by continuous ball milling at 500 rpm for 10 hours using a planetary ball mill (QM3SP2; Nanjing Instrument Company, China). The prepared powders were then loaded into a graphite mold with a diameter of 12.7 mm and hot-pressed using a ZT-40-20Y model hot press (Shanghai Chenhua Electric Furnace Co., China) under an axial pressure of 60 MPa at 973, 1023, and 1073 K for 2 minutes.

Structural characterization: The phase characterization was conducted using X-ray diffraction (XRD, Bruker D8 Advance) with Cu-Kα radiation, set at a scanning rate of 4° per minute. The fresh fracture surfaces and HNO_3-etched surfaces of the samples were analyzed by scanning electron microscopy (SEM, Hitachi Regulus 8100) to reveal surface morphology and grain size. The nanostructural features of $Mg_{3.4}Bi_{1.29}Sb_{0.7}Te_{0.01}$ sintered at 1073 K were observed using transmission electron microscopy (TEM, FEI Talos F200S).

Properties measurement: The Seebeck coefficient (S) and electrical conductivity (σ) were measured using the four-probe method (CTA-3, Beijing Cryostech Co.) under a helium atmosphere, in the temperature range of 300 to 773 K. The thermal conductivity (κ) was calculated using $\kappa = D\rho C_p$, where thermal diffusivity (D) was measured by an LFA 467 HT laser flash apparatus (NETZSCH, GmbH, Selb, Germany), specific heat capacity (C_p) was derived using the Dulong-Petit law, and density (ρ) was measured using the Archimedes method. Room-temperature carrier concentration (n) and mobility (μ) were characterized under a 1.5 T magnetic field using a physical property measurement system (Joule Yacht-HET-3RT). The van der Pauw method was used with a magnetic field up to ±0.5 T. n

and μ were calculated using $n = 1/(eR_H)$ and $\mu = \sigma R_H$, where e represents the electron charge.

DFT calculation: Density-functional theory (DFT) calculations were performed using the all electron projected augmented wave (PAW) method, as implemented in the Vienna Ab initio Simulation Package (VASP).[1-6] The generalized gradient approximation (GGA) with the fully relativistic Perdew-Burke-Ernzerhof (PBE) functional was employed to treat the exchange correlations.[7] To simulate the multiple doping envisaged by this work, quasi-random alloys were generated by minimizing the structural order derived from a 2×2×2 supercell containing 40 atoms using USPEX code, based on an evolutionary algorithm which features local optimization, real-space representation and flexible physically motivated variation operators.[8] All atoms in the as-built structures were allowed to relax in their geometric optimizations, during which the Brillouin zone was sampled by a 0.03 $Å^{-3}$ Monkhorst-Pack **k**-mesh, the valence wave functions were expanded in a plan-wave basis with a cut-off energy of 500 eV, and the convergence criteria were set to be 1×10^{-7} eV per electron and 1×10^{-3} eV·$Å^{-1}$ per unit cell. A denser 0.02 $Å^{-3}$ Monkhorst-Pack **k**-mesh was adopted for calculating density-of-state (DOS), and a line-mode **k**-path based on Brillouin path features indicated by the AFLOW framework was adopted for calculating band structures.[9, 10] Because Bi and Te are heavy elements, spin-orbital coupling (SOC) was considered by the non-self-consistent calculations.

Modelling. For calculation details of the single parabolic band (SPB) modeling, there are:[9, 11-14]

$$S(\eta) = \frac{k_B}{e} \cdot \left[\frac{\left(g + \frac{5}{2}\right) \cdot F_{g+\frac{3}{2}}(\eta)}{\left(g + \frac{3}{2}\right) \cdot F_{g+\frac{1}{2}}(\eta)} - \eta \right] \tag{S1-1}$$

$$n = \frac{1}{e \cdot R_H} = \frac{(2m^* \cdot k_B T)^{\frac{3}{2}}}{3\pi^2 \hbar^3} \cdot \frac{\left(g + \frac{3}{2}\right)^2 \cdot F_{g+\frac{1}{2}}^{\ 2}(\eta)}{(2g + \frac{3}{2}) \cdot F_{2g+\frac{1}{2}}(\eta)} \tag{S1-2}$$

$$\mu = \left[\frac{e\pi\hbar^4 \quad C_l}{\sqrt{2}(k_B T)^{\frac{3}{2}} E_{def}^{\ 2} (m^*)^{\frac{5}{2}}}\right] \frac{(2g + \frac{3}{2}) \cdot F_{2g+\frac{1}{2}}(\eta)}{\left(g + \frac{3}{2}\right)^2 \cdot F_{g+\frac{1}{2}}(\eta)} \tag{S1-3}$$

$$L = (\frac{k_B}{e})^2 \cdot \left\{ \frac{\left(g + \frac{7}{2}\right) \cdot F_{g+\frac{5}{2}}(\eta)}{\left(g + \frac{3}{2}\right) \cdot F_{g+\frac{1}{2}}(\eta)} - \left[\frac{\left(g + \frac{5}{2}\right) \cdot F_{g+\frac{3}{2}}(\eta)}{\left(g + \frac{3}{2}\right) \cdot F_{g+\frac{1}{2}}(\eta)} \right]^2 \right\} \tag{S1-4}$$

where η is the reduced Fermi level, k_B is the Boltzmann constant, g is the carrier scattering factor (g = -1/2 for acoustic phonon scattering), $\hbar$ is the reduced plank constant, C_l is the elastic constant for longitudinal vibrations, E_{def} is the deformation potential coefficient, m^* is the effective mass, and L is the Lorenz number. For C_l, there is:[11-14]

$$C_l = v_l^2 \rho \tag{S1-5}$$

where v_l is the longitudinal sound velocity. $F_i(\eta)$ is the Fermi integral expressed as:[11-14]

$$F_i(\eta) = \int_0^\infty \frac{x^i}{1 + e^{(x-\eta)}} dx \tag{S1-6}$$

uncertainty analysis: The accuracy and reliability of the three core parameters—electrical conductivity (σ), Seebeck coefficient (S), and thermal conductivity (κ)—are critical when evaluating the performance of thermoelectric materials. To ensure a comprehensive and precise assessment of the

fluctuation characteristics and measurement accuracy of these parameters, a rigorous approach involving multiple measurements was adopted. Each thermoelectric material sample underwent a minimum of three independent tests to guarantee consistency and reliability in the evaluation.

A series of precise measurements were conducted, revealing that the measured value of σ fluctuated around its average by approximately ±10%. This variability can be attributed to slight differences in the material preparation process, limitations in measurement equipment precision, and minor changes in environmental conditions. In contrast, the measured value of S demonstrated greater stability, with a smaller fluctuation of about ±2%, providing strong evidence of the high accuracy and excellent repeatability of this parameter. Similarly, the fluctuation range of the measured κ was approximately ±5%, further reflecting the high accuracy and repeatability of the entire measurement process. The remaining key performance parameters, such as the ZT value, were derived from the three core parameters mentioned above using specific formulas.

2. Supporting Figures

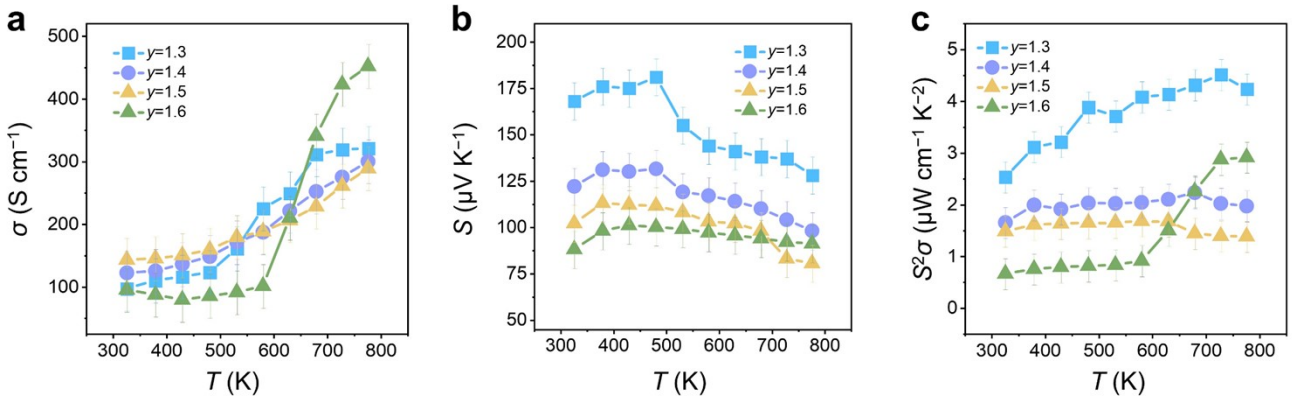

Figure S1. Temperature-dependent (**a**) electrical conductivity (σ), (**b**) Seebeck coefficient (S), and (**c**) power factor ($S^2\sigma$) of $Mg_{3.2}Bi_{2-y}Sb_y$.

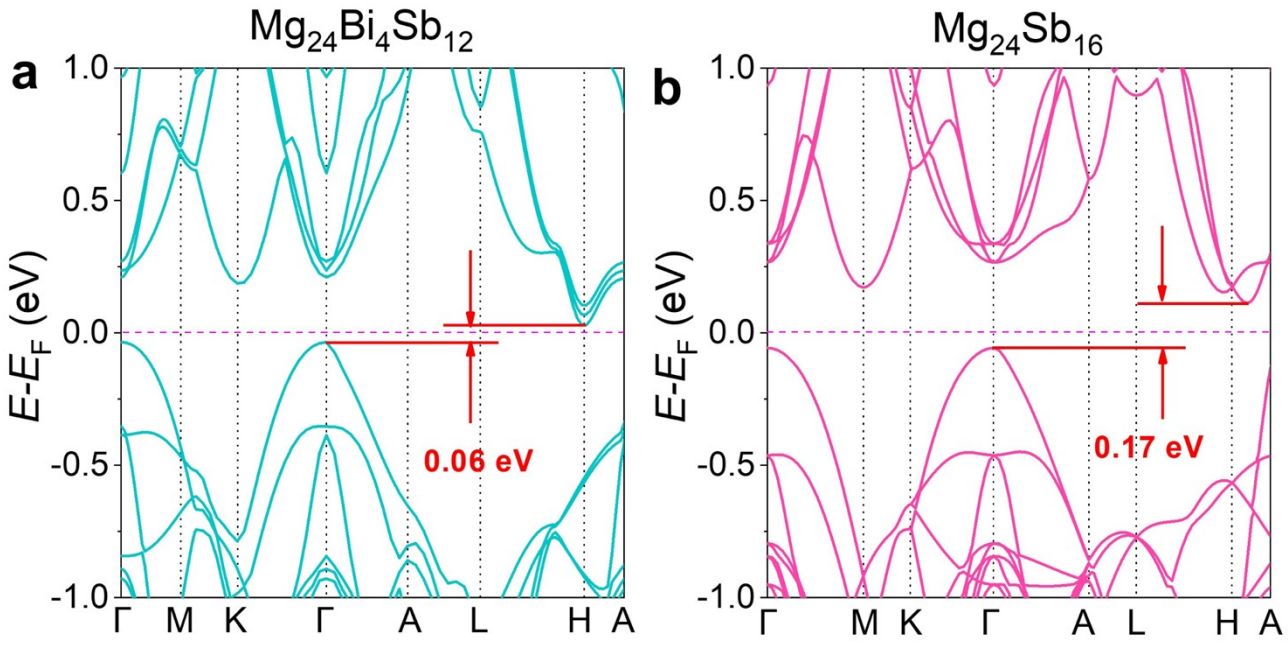

Figure S2. Calculated band structures of (**a**) $Mg_{24}Bi_4Sb_{12}$ and (**b**) $Mg_{24}Sb_{16}$.

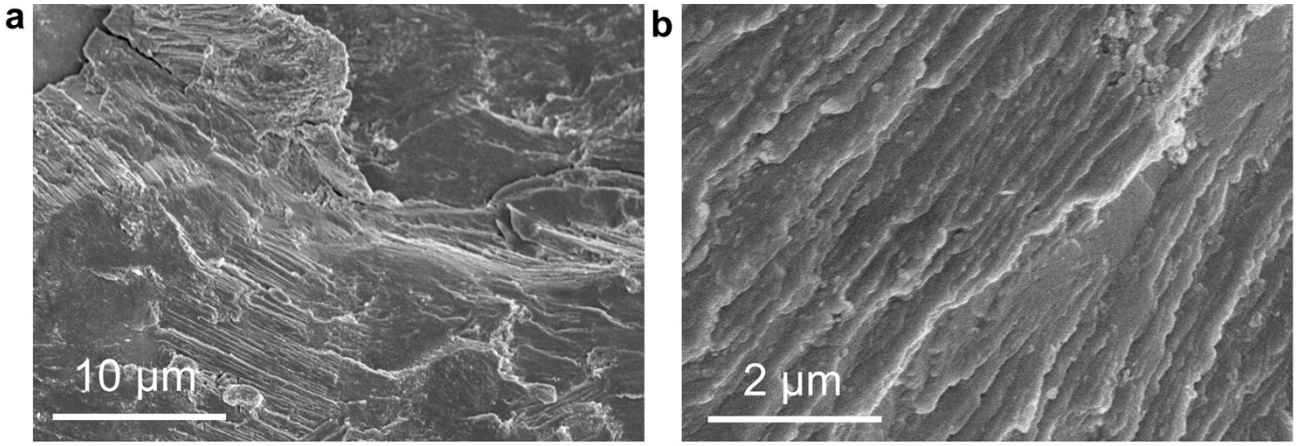

Figure S3. (**a-b**) Scanning electron microscopy (SEM) images of fractured surfaces of $Mg_{3.4}Bi_{1.29}Sb_{0.7}Te_{0.01}$.

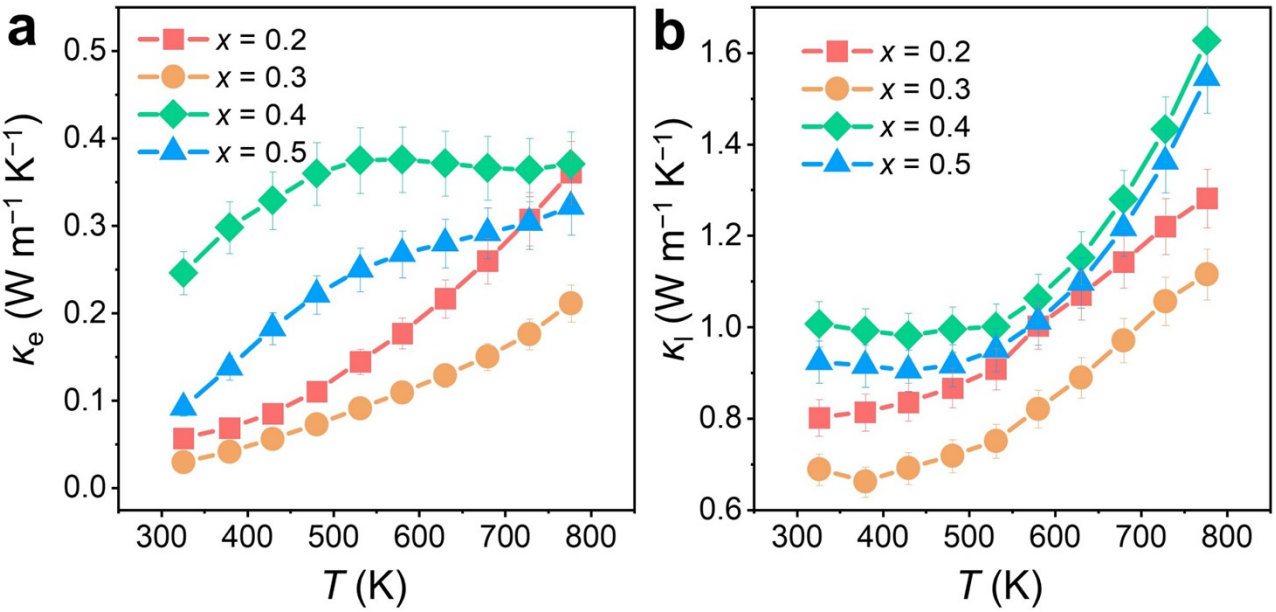

Figure S4. Temperature-dependent (**a**) electrical thermal conductivity (κ_e) and (**b**) lattice thermal conductivity (κ_l) of $Mg_{3+x}Bi_{1.29}Sb_{0.7}Te_{0.01}$.

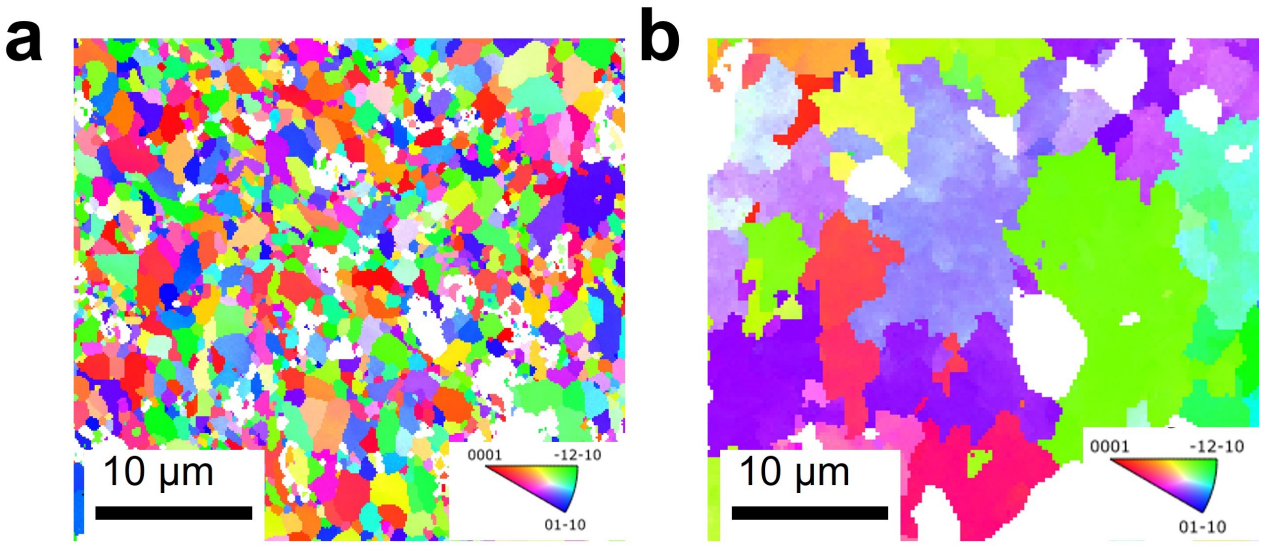

Figure S5. Electron Back Scatter Diffraction images of the samples for hot-pressing at (**a**) 973 K and (**b**) 1073 K.

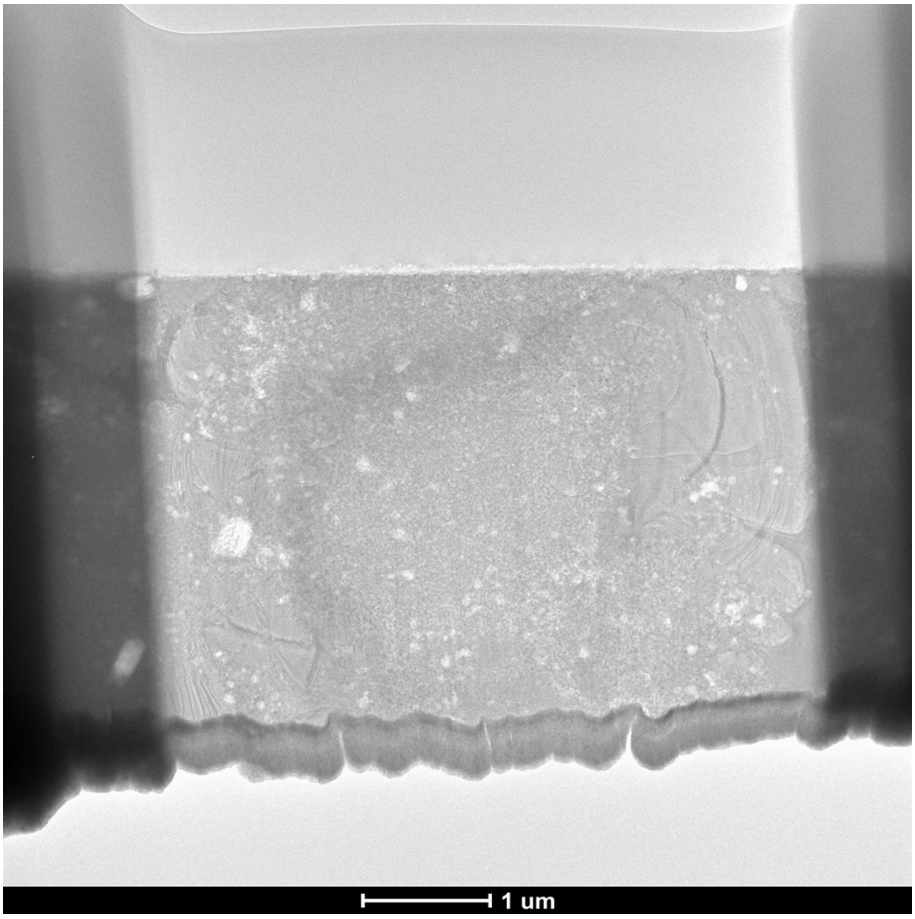

Figure S6. Transmission electron microscopy (TEM) image of the overview of the sample ($Mg_{3.4}Bi_{1.29}Sb_{0.7}Te_{0.01}$) prepared by the focused ion beam (FIB) technique.

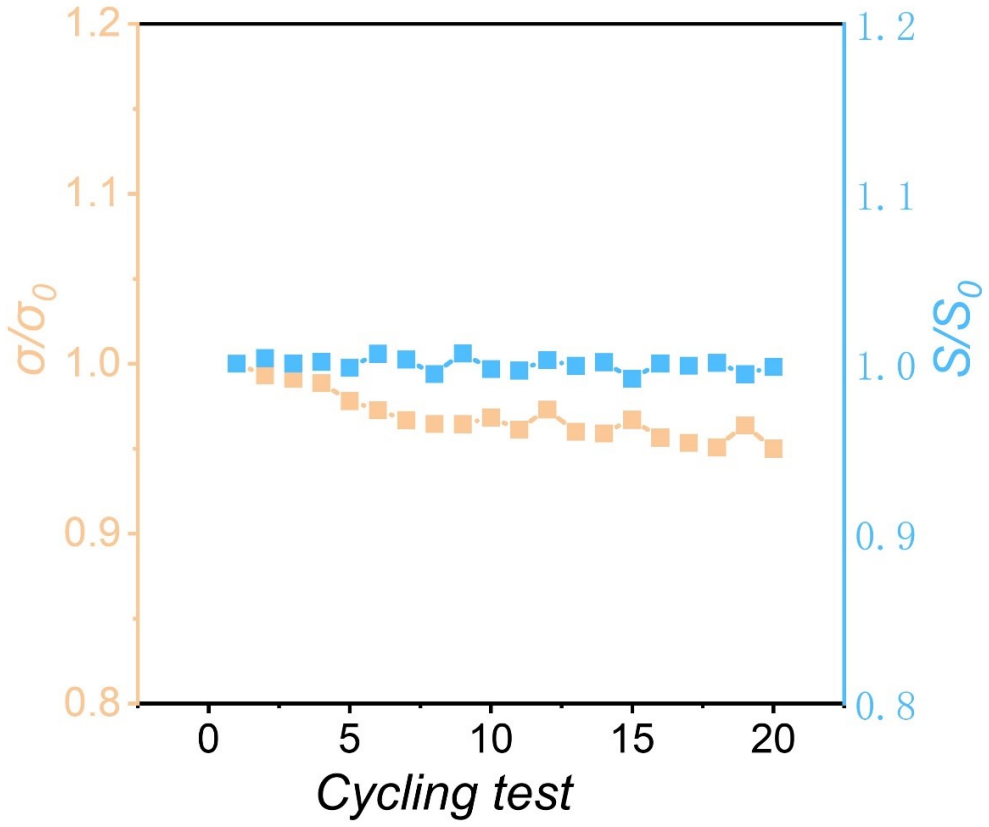

Figure S7. Stability of $\sigma(\sigma/\sigma_0)$ and $S(S/S_0)$ for $Mg_{3.4}Bi_{1.29}Sb_{0.7}Te_{0.01}$.

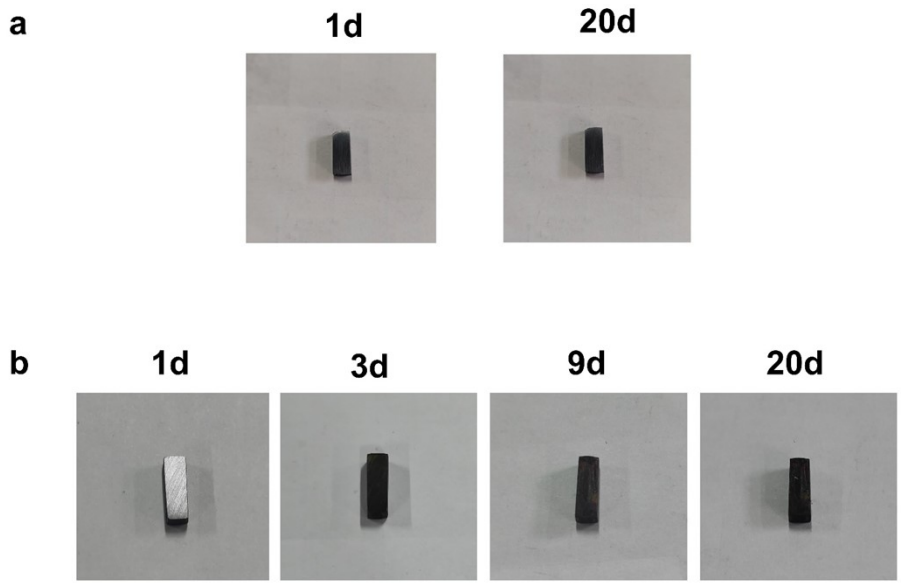

Figure S8. The optical images of $Mg_{3.4}Bi_{1.29}Sb_{0.7}Te_{0.01}$ samples. Samples were exposed to the ambient air (**a**) and water (**b**) with increasing days (d).

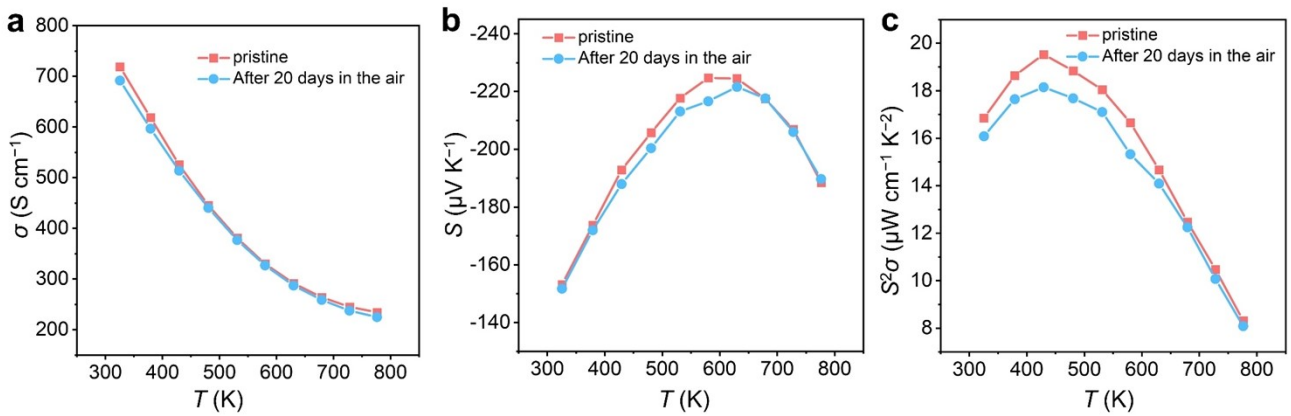

Figure S9. Thermoelectric performance of $Mg_{3.4}Bi_{1.29}Sb_{0.7}Te_{0.01}$ sintered at 1073 K in the ambient air. Temperature-dependent (**a**) electrical conductivity (σ) and (**b**) Seebeck coefficient (S), and (**c**) $S^2\sigma$.

Figure S10. Thermoelectric performance of $Mg_{3.4}Bi_{1.29}Sb_{0.7}Te_{0.01}$ sintered at 1073 K in the water. Temperature-dependent (**a**) electrical conductivity (σ) and (**b**) Seebeck coefficient (S), and (**c**) $S^2\sigma$.

3. Supporting Table

Table S1. Summary of thermoelectric performance of n-type Mg_3Bi_2-based thermoelectric materials.

Materials	Synthesis	300 K *ZT*	Peak *ZT*	$S^2\sigma$ (μW cm^{-1} K^{-2})	κ (W m^{-1} K^{-1})	Ref.
$Mg_{3.4}Bi_{1.29}Sb_{0.7}Te_{0.01}$	1073 K 2 min	0.5	0.9	18.03	1.07	**This work**
$Mg_{3.2}Bi_{1.298}Sb_{0.7}Te_{0.002}$	1053 K 2 min	0.75	0.92	~24	~0.91	[15]
$Mg_{3.05}(Bi_{0.7}Sb_{0.3})_{1.998}Te_{0.004}$	1073 K 20 min	0.6	1.1	~27	~1.18	[16]
$Mg_{3.2}Bi_{1.4}Sb_{0.595}Se_{0.005}$	1053 K 2 min	0.82	1.2	~26	~1.02	[17]
$Mg_{3.2}Bi_{1.29}Sb_{0.7}Te_{0.01}$	1053 K 2 min	0.5	1.07	~25	~1.1	[18]
$Mg_{3.2}Bi_{1.5}Sb_{0.48}Cu_{0.01}Te_{0.02}$	973 K 10 min	0.87	1.12	~28	~0.89	[19]
$Mg_{3.2}Bi_{1.395}Sb_{0.6}Te_{0.005}$	1073 K 20 min	0.68	1.05	~28.5	~1.15	[20]
$Mg_{3.17}Mn_{0.03}Bi_{1.29}Sb_{0.7}Te_{0.01}$	923 K 7 min	0.97	1.3	~28	~0.9	[21]
$Mg_{3.2}Nb_{0.01}Bi_{1.29}Sb_{0.7}Te_{0.01}$	923 K 7 min	1.02	1.15	~25	~0.92	[22]
$Mg_{3.2}Bi_{1.498}Sb_{0.7}Te_{0.002}Cu_{0.005}$	973 K 10 min	0.92	1.2	~28	~1.0	[23]

4. Raw data

Table S2. $Mg_{3+x}Bi_{1.29}Sb_{0.7}Te_{0.01}$ (x = 0.2, 0.3, 0.4, and 0.5).

Temperature (K)	σ (S cm^{-1})	S (μV K^{-1})	$S^2\sigma$ (μW cm^{-1} K^{-2})	κ (W m^{-1} K^{-1})	κ_e (W m^{-1} K^{-1})	κ_l (W m^{-1} K^{-1})	ZT
x=0.2							
325.67983	99.14822	138.3393	1.897475	0.80163	0.74479	0.05684	0.0770891
379.2596	103.71378	145.1916	2.1863488	0.81359	0.74517	0.06842	0.1019179
429.3422	114.27967	146.6469	2.4576201	0.83556	0.75043	0.08513	0.1262818
480.7089	132.05882	145.1302	2.7815252	0.86626	0.75583	0.11043	0.1543536
531.2776	154.94836	139.2956	3.006504	0.90852	0.76386	0.14466	0.1758121
580.2776	172.88296	137.0755	3.2484177	1.00254	0.82544	0.1771	0.1880208
630.1987	193.11607	132.4416	3.387406	1.07001	0.85342	0.21659	0.1995064
679.6201	213.1613	128.3093	3.5093334	1.14248	0.88258	0.2599	0.2087576
728.3436	233.86506	124.9631	3.6519845	1.22022	0.91256	0.30766	0.2179852
776.601	253.30545	117.8251	3.5165773	1.28174	0.92102	0.36072	0.213068
x=0.3							
325.67983	27.66273	-234.8181	1.52531	0.68828	0.65909	0.02919	0.07217
379.2596	43.92751	-244.0758	2.61689	0.66137	0.62028	0.04109	0.15006
429.3422	60.62462	-246.5925	3.68645	0.6908	0.6351	0.0557	0.22912
480.7089	76.60323	-252.0655	4.86714	0.71766	0.64526	0.0724	0.32601
531.2776	91.16984	-246.5472	5.54181	0.7502	0.65946	0.09074	0.39246
580.2776	102.80176	-236.3196	5.74116	0.82029	0.71142	0.10887	0.40613

630.1987	112.99993	-218.0237	5.37137	0.88889	0.76035	0.12854	0.38082
679.6201	122.2098	-195.9165	4.69081	0.9704	0.82032	0.15008	0.32852
728.3436	131.33644	-167.707	3.69392	1.05613	0.88033	0.1758	0.25475
776.601	142.59619	-135.0261	2.59982	1.11515	0.90403	0.21112	0.18105
***x*=0.4**							
325.67983	341.49705	-139.1917	6.61628	1.00636	0.76046	0.2459	0.21412
379.2596	423.28275	-170.495	12.30421	0.99123	0.69333	0.2979	0.47078
429.3422	460.44268	-186.1372	15.95299	0.9811	0.6567	0.329	0.69812
480.7089	461.23398	-198.1659	18.11253	0.99463	0.63503	0.3596	0.87539
531.2776	437.8347	-204.2575	18.26697	1.00034	0.62544	0.3749	0.97015
580.2776	403.38407	-210.3372	17.84642	1.0628	0.6872	0.3756	0.9744
630.1987	366.35713	-208.4499	15.91871	1.15148	0.78008	0.3714	0.87122
679.6201	333.42147	-204.7151	13.97312	1.27941	0.91341	0.366	0.74225
728.3436	307.0115	-197.2813	11.94886	1.43272	1.06882	0.3639	0.60744
776.601	287.62659	-181.6806	9.49393	1.62706	1.25656	0.3705	0.45315
***x*=0.5**							
325.67983	162.93712	-149.7409	3.65343	0.92316	0.83155	0.09161	0.12889
379.2596	216.78022	-171.4106	6.36935	0.91461	0.77708	0.13753	0.26412
429.3422	258.10228	-	8.74745	0.90463	0.72211	0.18252	0.41516

		184.0962					
480.7089	283.39233	-198.0874	11.11992	0.91562	0.69454	0.22108	0.58381
531.2776	291.08582	-203.4937	12.05377	0.9498	0.70012	0.24968	0.67424
580.2776	286.55348	-206.6899	12.24177	1.01151	0.74383	0.26768	0.70228
630.1987	275.48004	-205.7093	11.6573	1.09683	0.81711	0.27972	0.66979
679.6201	264.42015	-198.5017	10.41892	1.21633	0.92481	0.29152	0.58215
728.3436	253.77877	-187.5542	8.92707	1.36203	1.05876	0.30327	0.47737
776.601	247.88167	-172.2636	7.35583	1.54535	1.22369	0.32166	0.36966

Table S3. $Mg_{3.4}Bi_{1.29}Sb_{0.7}Te_{0.01}$ samples sintered at different temperatures of 923, 1023, and 1073 K

Temperature (K)	σ (S cm^{-1})	S (μV K^{-1})	$S^2\sigma$ (μW cm^{-1} K^{-2})	κ (W m^{-1} K^{-1})	κ_e (W m^{-1} K^{-1})	κ_l (W m^{-1} K^{-1})	ZT
sintered at 973 K							
325.67983	341.49705	-139.1917	6.61628	1.00636	0.76046	0.2459	0.21412
379.2596	423.28275	-170.495	12.30421	0.99123	0.69333	0.2979	0.47078
429.3422	460.44268	-186.1372	15.95299	0.9812	0.6567	0.3291	0.69812
480.7089	461.23398	-198.1659	18.11253	0.99463	0.63503	0.3596	0.87539
531.2776	437.8347	-204.2575	18.26697	1.00034	0.62544	0.3749	0.97015
580.2776	403.38407	-210.3372	17.84642	1.0628	0.6872	0.3756	0.9744
630.1987	366.35713	-208.4499	15.91871	1.15148	0.78008	0.3714	0.87122
679.6201	333.42147	-204.7151	13.97312	1.27941	0.91341	0.366	0.74225
728.3436	307.0115	-197.2813	11.94886	1.43272	1.06882	0.3639	0.60744
776.601	287.62659	-181.6806	9.49393	1.62706	1.25656	0.3705	0.45315
sintered at 1023 K							
325.67983	712.17615	-150.8454	16.20511	1.11304	0.71244	0.4006	0.47314
379.2596	608.48607	-171.5256	17.90229	1.0682	0.6836	0.3846	0.63433
429.3422	524.55357	-185.5032	18.05064	1.03473	0.66533	0.3694	0.74885
480.7089	449.89781	-197.7618	17.59539	1.01772	0.66682	0.3509	0.83048
531.2776	391.25667	-209.2352	17.12898	1.01901	0.68551	0.3335	0.88998
580.2776	345.04092	-211.8811	15.49013	1.04042	0.71952	0.3209	0.86161
630.1987	307.52766	-211.9032	13.8089	1.08719	0.77639	0.3108	0.79792
679.6201	279.73804	-208.3014	12.13769	1.15952	0.85352	0.306	0.70973
728.3436	259.48819	-196.8167	10.05175	1.25933	0.95163	0.3077	0.58011
776.601	246.31798	-180.2378	8.00181	1.37667	1.05887	0.3178	0.45144

sintered at 1073 K							
325.67983	718.45055	-153.128	16.84637	1.2222	0.8427	0.3795	0.45104
379.2596	618.23649	-173.6059	18.63303	1.16109	0.79369	0.3674	0.60535
429.3422	525.23702	-192.7955	19.52312	1.11458	0.76868	0.3459	0.75198
480.7089	445.20821	-205.6814	18.83447	1.08279	0.75789	0.3249	0.83762
531.2776	380.48723	-217.7043	18.03325	1.07423	0.77063	0.3036	0.89343
580.2776	329.67272	-224.712	16.64697	1.09244	0.80644	0.286	0.88712
630.1987	291.10815	-224.4565	14.66623	1.13599	0.86139	0.2746	0.81687
679.6201	263.59879	-217.4587	12.46514	1.21184	0.94204	0.2698	0.7017
728.3436	244.65485	-206.8345	10.46646	1.31688	1.04598	0.2709	0.58193
776.601	233.92558	-188.4561	8.30803	1.45985	1.17805	0.2818	0.44489

References

1. G. Kresse and J. Hafner, *Phys. Rev. B*, 1994, **49**, 14251-14269.
2. G. Kresse and J. Hafner, *Phys. Rev. B*, 1993, **47**, 558-561.
3. G. Kresse and J. Furthmüller, *Comp. Mater. Sci.*, 1996, **6**, 15-50.
4. G. Kresse and J. Hafner, *J. Phys. Condens. Mat.*, 1994, **6**, 8245-8257.
5. G. Kresse and J. Furthmüller, *Phys. Rev. B*, 1996, **54**, 11169-11186.
6. G. Kresse and D. Joubert, *Phys. Rev. B*, 1999, **59**, 1758-1775.
7. J. P. Perdew, K. Burke and M. Ernzerhof, *Phys. Rev. Lett.*, 1996, **77**, 3865-3868.
8. A. R. Oganov and C. W. Glass, *J. Chem. Phys.*, 2006, **124**, 244704.
9. W. Setyawan and S. Curtarolo, *Comp. Mater. Sci.*, 2010, **49**, 299-312.
10. F. Tran and P. Blaha, *Phys. Rev. Lett.*, 2009, **102**, 226401.
11. X. L. Shi, K. Zheng, M. Hong, W. D. Liu, R. Moshwan, Y. Wang, X.-L. Qu, Z. G. Chen and J. Zou, *Chem. Sci.*, 2018, **9**, 7376-7389.
12. X. Shi, A. Wu, T. Feng, K. Zheng, W. Liu, Q. Sun, M. Hong, S. T. Pantelides, Z. G. Chen and J. Zou, *Adv. Energy Mater.*, 2019, **9**, 1803242.
13. X. Shi, A. Wu, W. Liu, R. Moshwan, Y. Wang, Z.-G. Chen and J. Zou, *ACS Nano*, 2018, **12**, 11417-11425.
14. M. Jin, X.-L. Shi, T. Feng, W. Liu, H. Feng, S. T. Pantelides, J. Jiang, Y. Chen, Y. Du, J. Zou and Z.-G. Chen, *ACS Appl. Mater. Interfaces*, 2019, **11**, 8051-8059.
15. J. Mao, H. Zhu, Z. Ding, Z. Liu, G. A. Gamage, G. Chen and Z. Ren, *Science*, 2019, **365**, 495-498.
16. K. Imasato, S. D. Kang and G. J. Snyder, *Energy Environ. Sci.*, 2019, **12**, 965-971.

17. X. Mo, J. Liao, G. Yuan, S. Zhu, X. Lei, L. Huang, Q. Zhang, C. Wang and Z. Ren, *J. Magnes. Alloy.*, 2022, **10**, 1024-1032.
18. Z. Liang, C. Xu, H. Shang, Q. Zhu, F. Ding, J. Mao and Z. Ren, *Mater. Today Phys.*, 2021, **19**, 100413.
19. Z. Liu, W. Gao, H. Oshima, K. Nagase, C.-H. Lee and T. Mori, *Nat. Commun.*, 2022, **13**, 1120.
20. N. Qu, Y. Zhu, J. Zhu, K. Yu, F. Guo, Z. Liu, Q. Zhang, W. Cai and J. Sui, *J. Magnes. Alloy.*, 2024, **12**, 4538-4546.
21. K. Yang, X. Li, C. Sun, W. Song, W. Zhao and Q. Zhang, *Adv. Funct. Mater.*, 2024, **34**, 2315886.
22. X. Li, C. Sun, K. Yang, D. Liang, X. Ye, W. Song, W. Xu, W. Zhao and Q. Zhang, *Small*, 2024, **20**, 2311478.
23. H. Cho, S. Y. Back, N. Sato, Z. Liu, W. Gao, L. Wang, H. D. Nguyen, N. Kawamoto and T. Mori, *Adv. Funct. Mater.*, 2024, **34**, 2407017.